Luminal Ca^{2+} dynamics during IP_3R mediated signals

2016 Phys. Biol. 13 036006

(http://iopscience.iop.org/1478-3975/13/3/036006)

Physical Biology

PAPER

Luminal Ca^{2+} dynamics during IP_3R mediated signals

Lucia F Lopez and Silvina Ponce Dawson

DF, FCEN-UBA, Argentina
IFIBA, CONICET, Argentina

E-mail: luhalac@df.uba.ar

RECEIVED
3 March 2016

REVISED
30 April 2016

ACCEPTED FOR PUBLICATION
12 May 2016

PUBLISHED
27 May 2016

Keywords: luminal calcium, cytosolic calcium, microscopy, buffers

Supplementary material for this article is available online

Abstract

The role of cytosolic Ca^{2+} on the kinetics of Inositol 1,4,5-triphosphate receptors (IP_3Rs) and on the dynamics of IP_3R-mediated Ca^{2+} signals has been studied at large both experimentally and by modeling. The role of luminal Ca^{2+} has not been investigated with that much detail although it has been found that it is relevant for signal termination in the case of Ca^{2+} release through ryanodine receptors. In this work we present the results of observing the dynamics of luminal and cytosolic Ca^{2+} simultaneously in *Xenopus laevis* oocytes. Combining observations and modeling we conclude that there is a rapid mechanism that guarantees the availability of free Ca^{2+} in the lumen even when a relatively large Ca^{2+} release is evoked. Comparing the dynamics of cytosolic and luminal Ca^{2+} during a release, we estimate that they are consistent with a 80% of luminal Ca^{2+} being buffered. The rapid availability of free luminal Ca^{2+} correlates with the observation that the lumen occupies a considerable volume in several regions across the images.

1. Introduction

Ca^{2+} signals are ubiquitous. They are involved in the regulation of processes as diverse as fertilization, cell motility and cell death, among many others [1, 2]. One of the key features on which the versatility of the Ca^{2+} signaling toolkit relies is the variety of spatio-temporal distributions that the cytosolic Ca^{2+} concentration can display. Ca^{2+} release from internal stores, such as the endoplasmic or sarcoplasmic reticulum (ER and SR, respectively), is a universal feature of Ca^{2+} signals [3]. In particular, Ca^{2+} release through inositol 1,4,5-trisphosphate receptors (IP_3Rs) [4] is a primary component of them [5]. The role of the released (cytosolic) Ca^{2+} on the induction of further release (through the mechanisms known as Ca^{2+}-induced-Ca^{2+}-release or CICR) is well-known in IP_3R-mediated Ca^{2+} signals [6]. Namely, cytosolic Ca^{2+} plays a dual role on IP_3Rs leading to their opening at moderate concentrations and to their inhibition at very large ones [4, 7]. Thus, the initial increase in cytosolic Ca^{2+} due to its release through an open IP_3R induces the opening of its neighboring IP_3Rs. A variety of signals then arises [8, 9] depending on the interplay between the spatial arrangement of the channels [10, 11], the (basal) cytosolic Ca^{2+} level [12] and the Ca^{2+}-trapping or removing mechanisms [13–15] at work. The role of luminal Ca^{2+} on the kinetics of IP_3Rs [16, 17] or on the dynamics of IP_3R-mediated Ca^{2+} signals [18] has not been studied as much. This is different from studies in myocytes, where Ca^{2+} is released from the SR through ryanodine receptors (RyR), and where it has been determined that luminal Ca^{2+} is directly implicated in the termination of Ca^{2+} signals, particularly, in cardiomyocytes [19, 20]. Furthermore, it has recently been shown that the gate of some subtype of RyRs senses luminal Ca^{2+}, explaining in this way the initiation of spontaneous Ca^{2+} waves and Ca^{2+}-triggered arrhythmias [21]. Despite the analogy between RyRs and IP_3Rs, the characterization of luminal Ca^{2+} sensors on IP_3Rs [22, 23] and the evidence that IP_3R-mediated Ca^{2+} signals depend on the content of intracellular stores [18, 24] the role of luminal Ca^{2+} on the dynamics of IP_3R-mediated signals is still unclear [7, 25]. It is thus of interest to investigate the role of luminal Ca^{2+} on IP_3Rs and IP_3R-mediated Ca^{2+} signals.

In this paper we present a protocol to observe luminal Ca^{2+} in *Xenopus laevis* oocytes. To this end, we use the low affinity dye, Fluo-5N AM, which has

been proved to be a good reporter of luminal Ca^{2+} in other cell types [26]. To the best of our knowledge, this is the first time that the dynamics of luminal Ca^{2+} is observed in this model system that is particularly useful to study IP_3R-mediated Ca^{2+} signals since Ca^{2+} release from the ER occurs only through IP_3Rs (of a particular subtype). Furthermore, it is a system where the full range of signals, from local to global ones, has been observed. After testing the protocol and proving that the dye is indeed marking luminal Ca^{2+}, we study the spatial distribution of the latter and the dynamics of its depletion after an $InsP_3$-releasing UV exposure [12, 27]. We observe that the dynamics of luminal Ca^{2+} depletion is slower than what would be expected. This is consistent with having a Ca^{2+} 'store' in the ER that is continuously supplying new free Ca^{2+} as needed when there is release into the cytosol. The possibility that this refilling mechanism be more relevant in oocytes than in other cell types, such as muscle, where luminal Ca^{2+} depletion could be observed during local signals known as sparks [28] could be related to the different volume that the lumen occupies in each cell type. In fact, visualizing luminal Ca^{2+} simultaneously with a dye that marks the surface of the ER or with another that marks cytosolic Ca^{2+} we observe that the lumen occupies a relatively large portion of the observed region. This fast supply of Ca^{2+} can be provided by 'buffers' present in the lumen. We corroborate the existence of this fast supply of Ca^{2+} upon Ca^{2+} release through IP_3Rs and we quantify the fraction of luminal Ca^{2+} that is buffered with experiments in which we observe luminal and cytosolic Ca^{2+} simultaneously. For the latter we use the dye, Rhod-2, at a concentration that provides the same signal detectability as the more commonly used Fluo-based Ca^{2+} dyes. This choice of concentration could be made based on our recently introduced method [29] that allows a quantitative comparison in terms of detectability of Ca^{2+}-imaging experiments.

2. Materials and methods

2.1. Fluo-5N AM

The dye Fluo-5N AM is the AM ester version of Fluo-5N, a low affinity ($K_d = 90\ \mu M$) analog of Fluo-4. The excitation and emission spectra of the dye are similar to those of Fluo-4. Fluo-5N AM is dissolved in Pluronic F-127 to a 4 mM concentration and then re diluted in Barth's solution. Instead of waiting for the AM ester to permeate the cell membrane, Fluo-5N AM is injected. Fluo-5N AM was used to probe luminal Ca^{2+}, its concentration in the cell was varied for the different experiments.

2.2. Oocyte preparation

Experiments were performed on immature and defolliculated oocytes from *Xenopus laevis*. Oocytes were loaded by intracellular micro injection with different compounds. Recordings were made at room temperature. Three Ca^{2+} dyes (Fluo-5N AM, Rhod-2, Fluo-4) and a lipophilic tracer (Dil) were used for the different experiments. Caged $InsP_3$ (D-Myo-Inositol 1,4,5-Triphosphate,P4(5)-(1-(2-Nitrophenyl)ethyl) Ester) was used to induce IP_3R opening. The exogenous Ca^{2+} buffers EGTA and BAPTA were also used to buffer cytosolic Ca^{2+}. In all the experiments Fluo-5N AM was injected at least 3 hs before the acquisition (with the exception of those that were done to monitor how long it takes for Fluo-5N AM to enter the ER) and Dil was injected 12 hs before the acquisition. Final intracellular concentrations of Fluo-4 and Rhod-2 were 37 μM and 92 μM respectively assuming 1 μl cytosolic volume [30] for the experiments of section 3.2. In the experiments of sections 3.1, 3.2 and 3.3 [Fluo-5N AM] was 92 μM. For the experiments presented in figure 5 of section 3.4 the final intracellular concentrations of Fluo-5N AM and caged $InsP_3$ were 74 μM and 9 μM. For the experiments presented in figure 6 of the same section the final intracellular concentrations of Fluo-5N AM, Rhod-2 and caged $InsP_3$ were 15 μM, 68 μM and 7 μM respectively. Fluo-5N AM, Fluo-4, Rhod-2, caged $InsP_3$, Dil and BAPTA were from Molecular Probes Inc.; EGTA was from Sigma Aldrich.

2.3. Confocal microscopy

Confocal imaging was performed using a spectral confocal scanning microscope Olympus FluoView1000 that has a scan unit connected to an inverted microscope IX81. Flash photolysis of the caged compound was made with a mercury lamp that comes with the microscope using the modification introduced in [27]. Fluo-5N AM and Fluo-4 were excited using the 488 nm line of a multiline Argon laser, Dil and Rhod-2 were excited using a He-Ne laser (543 nm). Both lasers were focused on the oocyte with a 60× oil immersion objective (NA 1.35). The emitted fluorescence was detected in the 500–600 nm and the 600–630 nm range respectively with PMT detectors.

2.4. Image acquisition

Frames were acquired either using 1X zoom or 10X zoom. For the loading experiments presented in section 3.1 a 512 × 512 pixels frame was acquired with 1X zoom resulting in a scanned region inside the oocyte of 210 × 210 μm^2. Frames were acquired every 30, 60 or 120 seconds. For the experiments shown in sections 3.2 and 3.3 a 512 × 512 pixels frame was acquired with 10X zoom resulting in a scanned region inside the oocyte of 21 × 21 μm^2. The experiments presented in figure 5 of section 3.4 were performed acquiring 256 × 256 pixels frames with 1X zoom (105 × 105 μm^2 region inside the oocyte). Frames were acquired every second for these experiments. The experiments presented in figure 6 of section 3.4 were performed acquiring 100 × 100

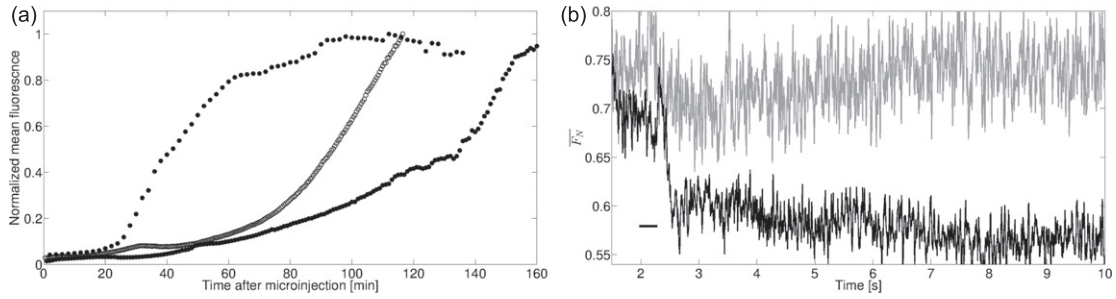

Figure 1. (A) Fluo-5N AM fluorescence evolution after the injection for three different oocytes. Plots represent the normalized mean fluorescence over time during the loading of the dye into the ER lumen. [Fluo-5N AM] = 74 μM (empty circles), [Fluo-5N AM] = 92 μM (filled circles). (B) Time course of fluorescence averaged (and normalized) over a 250 pixel line for a short UV exposure (indicated by a small black bar at the bottom). The gray line is an experiment with Fluo-5N AM and the black line is the same experiment but also with caged $InsP_3$.

pixels frames with 1X zoom (41 × 41 μm^2 region inside the oocyte). Frames were acquired every 0.165 s for these experiments. For the experiments performed in the linescan imaging mode (shown in figure 1(b) of section 3.1), linescan images were obtained by scanning along a fixed line (250 pixels) inside the oocyte with 10X zoom. The acquisition rate was fixed at 10 μs per pixel resulting in a scan rate of 3.26 s per line.

2.5. Image analysis

All images were analyzed using routines written in MATLAB. In the experiments performed using both spectral channels, we use a linear unmixing method to minimize the effect of spectral bleedthrough. If we call $F(\vec{r}_i, t)$ the fluorescence intensity in pixel $\vec{r}_i$ at time t we define $\overline{F}$ (averaged fluorescence over a line) and $\langle F \rangle$ (mean fluorescence over a frame) as

$$\overline{F} = \sum_{\vec{r}_i \in \text{line}} \frac{F(\vec{r}_i, t)}{\#\vec{r}_i}, \tag{1}$$

$$\langle F \rangle = \sum_{\vec{r}_i \in \text{frame}} \frac{F(\vec{r}_i, t)}{\#\vec{r}_i}. \tag{2}$$

And the corresponding basal values before the time, t_{UV}, of the stimulus as

$$\overline{F_b} = \sum_{\substack{\vec{r}_i \in \text{line} \\ t < t_{UV}}} \frac{F(\vec{r}_i, t)}{\#\vec{r}_i \# t}, \tag{3}$$

$$\langle F_b \rangle = \sum_{\substack{\vec{r}_i \in \text{frame} \\ t < t_{UV}}} \frac{F(\vec{r}_i, t)}{\#\vec{r}_i \# t}. \tag{4}$$

In some signaling experiments, we present the data normalized to these basal values. We define the normalized values $\overline{F_N}$ and $\langle F_N \rangle$ as

$$\overline{F_N} = \frac{\overline{F}}{\overline{F_b}}, \tag{5}$$

$$\langle F_N \rangle = \frac{\langle F \rangle}{\langle F_b \rangle}. \tag{6}$$

A threshold was applied to some images in order to count the pixels from the different fluorescence channels.

2.6. Model for Ca^{2+} variations and fluorescence

We present a simple model that describes the key features of cytosolic and luminal Ca^{2+} dynamics. Here, Ca is the free Ca^{2+}, CaD is Ca^{2+} bound to dye and CaB is Ca^{2+} bound to buffers. We consider that both cytosolic and luminal Ca^{2+} can be found in these three forms. The total Ca^{2+} concentration in either the ER lumen or the cytosol is then $[Ca_T^{(L,c)}] = [CaB^{(L,c)}] + [CaD^{(L,c)}] + [Ca^{(L,c)}]$ where the superscripts (L, c) indicate luminal or cytosolic Ca^{2+}, respectively. In order to compare with the experimental observations, we average the concentrations over a luminal (V_L) or cytosolic (V_c) volume that does not necessarily embrace the whole volume of each of these stores. We define the time derivative of the average total Ca^{2+} concentration in either of these volumes as

$$\frac{\partial \langle [Ca_T^{(L,c)}] \rangle}{\partial t} \equiv \frac{1}{V_{L,c}} \int_{V_{L,c}} \frac{\partial [Ca_T^{(L,c)}]}{\partial t} d^3r, \tag{7}$$

with equivalent expressions for the other concentrations ($[CaB^{(L,c)}]$, $[CaD^{(L,c)}]$ and $[Ca^{(L,c)}]$). The (partial) volumes, V_L or V_c, are limited by a common area, A, that corresponds to the membrane of the ER. We refer to V_L or V_c as 'partial' volumes because we want to connect the model with the observations and the experimental images do not embrace the whole cell. Thus, the observed volumes are partly surrounded by another area that is artifactual which is determined by the finite size of the image (see Supporting Material for more details). During the early stages of an IP_3R-mediated Ca^{2+} signal the average total Ca^{2+} concentration in V_L or in V_c varies mainly due to the exchange through the IP_3Rs that are located on the common area A. In our model we then neglect the diffusive flow of total Ca^{2+} through the other (artifactual) area that limits V_L or V_c. We are also neglecting the effect of Ca^{2+} pumps and Ca^{2+} leak during the early stages of the Ca^{2+} release because we assume it occurs on a much slower time-scale. In this way the total luminal [Ca^{2+}] dynamics at the beginning of the IP_3R-mediated Ca^{2+} release is modeled as

$$\frac{\partial\langle[\mathrm{Ca}_{\mathrm{T}}^{(\mathrm{L})}]\rangle}{\partial t}\Big|_{\mathrm{rel}} \approx -\frac{1}{V_{\mathrm{L}}}\left(\int_A \vec{j}_{\mathrm{IP_3R}}\cdot\vec{\mathrm{d}S}\right) \equiv -J_{\mathrm{IP_3R}}, \quad (8)$$

where $\vec{j}_{\mathrm{IP_3R}}$ is the Ca^{2+} flow through the open IP_3Rs located on A and where the label 'rel' refers to the fact that we are modeling the dynamics during a Ca^{2+} release event. The same event but viewed from the cytosol represents an increase in the total cytosolic $[Ca^{2+}]$ which we model as:

$$\frac{\partial\langle[\mathrm{Ca}_{\mathrm{T}}^{(\mathrm{c})}]\rangle}{\partial t}\Big|_{\mathrm{rel}} \approx \frac{1}{V_{\mathrm{c}}}\left(\int_A \vec{j}_{\mathrm{IP_3R}}\cdot\vec{\mathrm{d}S}\right). \quad (9)$$

Using (8)–(9) we relate variations in total $[Ca^{2+}]$ during a release event at both sides of the ER membrane as

$$\begin{aligned}\frac{\partial\langle[\mathrm{Ca}_{\mathrm{T}}^{(\mathrm{L})}]\rangle}{\partial t}\Big|_{\mathrm{rel}} &= \frac{\partial\langle[\mathrm{CaD}^{(\mathrm{L})}]\rangle}{\partial t} \\ &\quad + \frac{\partial}{\partial t}(\langle[\mathrm{Ca}^{\mathrm{L}}]\rangle + \langle[\mathrm{CaB}^{\mathrm{L}}]\rangle) \\ &\approx -\frac{V_{\mathrm{c}}}{V_{\mathrm{L}}}\frac{\partial\langle[\mathrm{Ca}_{\mathrm{T}}^{\mathrm{c}}]\rangle}{\partial t}\Big|_{\mathrm{rel}}.\end{aligned} \quad (10)$$

To relate the model with our experimental observations we use the method introduced in [29] that allows to link variations in the collected fluorescence from a single wavelength Ca^{2+} dye to the underlying Ca^{2+}-bound dye concentration. If we consider a fluorescence variation (with respect to a basal value F_{b}) for a given Ca^{2+} dye, D, we have (see Supplementary Material for more details):

$$\begin{aligned}\frac{1}{\langle F_{\mathrm{b}}\rangle}\frac{\Delta\langle F\rangle}{\Delta t} &= \frac{\left(1-\frac{q_2}{q_1}\right)}{\left(1-\frac{q_2}{q_1}\right)[\mathrm{CaD_b}]+\frac{q_2}{q_1}[D_{\mathrm{T}}]} \\ &\quad \times \frac{\Delta\langle[\mathrm{CaD}]\rangle}{\Delta t},\end{aligned} \quad (11)$$

where F_{b} and F are the fluorescence coming from the dye, D, ΔF is the fluorescence variation $F - F_{\mathrm{b}}$ that occurs during the time interval Δt, q_2/q_1 is the ratio of the number of photons per emitting molecule that reach the detector during the acquisition time for the Ca^{2+}-bound and Ca^{2+}-free forms of the dye, $[D_{\mathrm{T}}]$ is the total dye concentration and $[\mathrm{CaD_b}]$ is the basal Ca^{2+}-bound dye concentration, both concentrations in the region of interest (V_{L} or V_{c} depending on the dye). As done in [29] we use $q_2/q_1 = 0.07$ for Rhod-2 and, for Fluo-5N AM, we use the same value that we used for Fluo-4, $q_2/q_1 = 0.025$. We approximate $\Delta\langle[\mathrm{CaD}^{(\mathrm{L,c})}]\rangle/\Delta t \approx \partial\langle[\mathrm{CaD}^{(\mathrm{L,c})}]\rangle/\partial t$ with the latter given by the equivalent of 7 for CaD. This identification is applicable provided that $[\mathrm{CaD_b}] = [\mathrm{CaD}]$ right before the application of the UV exposure that elicits the change in fluorescence. The fact that 11 is an equation for a ratio of averages allows us to relate the average of the fluorescence (2) which is performed over the whole frame with that of [CaD] which is given by an integral over V_{L} or V_{c}. We estimate $[\mathrm{CaD_b}]$ by considering that Ca^{2+} and the dye are in equilibrium:

$$[\mathrm{CaD_b}] = \frac{[D_{\mathrm{T}}][\mathrm{Ca_b}]}{[\mathrm{Ca_b}]+K_{\mathrm{D}}}, \quad (12)$$

with $[D_{\mathrm{T}}] = [\mathrm{Rhod}-2]$, $K_{\mathrm{D}} = 2\ \mu\mathrm{M}$ and $[\mathrm{Ca_b^c}] = 100$ nM for the cytosol and $[D_{\mathrm{T}}] = [\mathrm{Fluo}-5\mathrm{N\ AM}]$, $K_{\mathrm{D}} = 90\ \mu\mathrm{M}$ and $[\mathrm{Ca_b^L}] = 200\ \mu\mathrm{M}$ [31] in the lumen of the ER.

3. Experimental results

3.1. Intracellular loading of the luminal dye

The fluorescence coming from a region of the oocyte was recorded for up to 2 hs after having injected Fluo-5N AM. The mean fluorescence $\langle F\rangle$ was computed for every frame (and then normalized to the maximum value).

The fluorescence is expected to increase as the dye is being loaded into the ER and binds luminal Ca^{2+}. The data from three different oocytes is shown in figure 1(a). The disparity between the three plots can be attributed to the fact that the recordings were made in three different oocytes and in arbitrarily chosen regions inside those cells. The imaging region that we sample in each case does not necessarily have the same amount of luminal pixels. It takes on the order of 60 min or longer for the fluorescence to increase noticeably in all cases. This delay can be the time it takes for the dye to enter the ER and report luminal Ca^{2+} or there could be an experimental artifact and Fluo-5N AM is sensing cytosolic Ca^{2+}. To rule the latter out, we measured the Fluo-5N AM fluorescence in the presence of increasing concentrations of two cytosolic Ca^{2+} buffers, EGTA [32] and BAPTA, and did not observe any difference (see figures S2A and S2B of the Supporting Material). If Fluo-5N AM was binding cytosolic Ca^{2+}, then its fluorescence should significantly decrease in the presence of EGTA or BAPTA. The results suggest that Fluo-5N AM is reporting Ca^{2+} inside the ER (or another reservoir where $[Ca^{2+}]$ is higher than in the cytosol).

To provide further support for our conclusion that Fluo-5N AM is monitoring the concentration of luminal Ca^{2+} we present in figure 1(b) the results of an experiment where we compare the time course of the normalized average Fluo-5N AM fluorescence obtained in the linescan imaging mode for a control oocyte (without caged $InsP_3$) and for an oocyte with 9 μM of caged $InsP_3$. The short bar at the bottom of the plot indicates the UV photolysis flash. The gray line is the control oocyte where the fluorescence remains at the same level before and after the UV stimulus. The black line (oocyte with caged $InsP_3$) on the other hand presents a marked decrease after the stimulus is delivered. The steep and fast decrease indicates that we are not observing bleaching of the dye but instead a more abrupt process. When the caged $InsP_3$ is photoreleased, there is a localized depletion of luminal Ca^{2+} and this is reflected in a lower concentration of Ca^{2+}

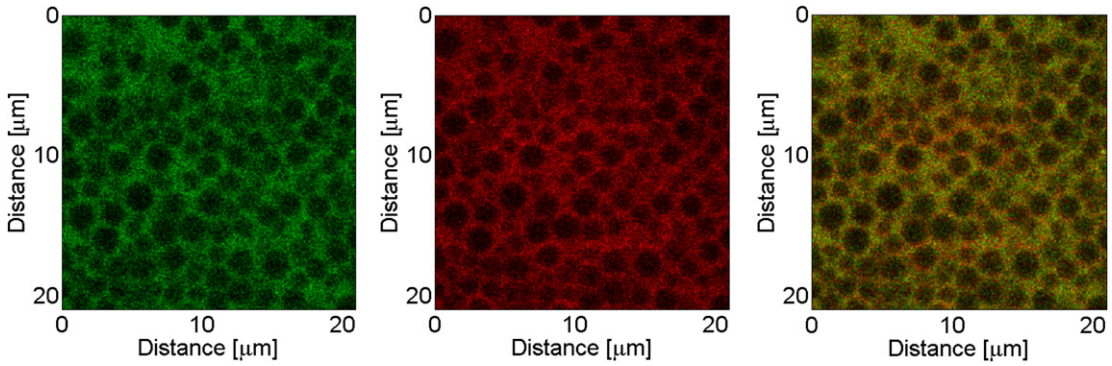

Figure 2. Spatial distribution of 2 cytosolic dyes: Fluo-4 (green channel) and Rhod-2 (red channel) inside the oocyte. Superimposed image of both distributions (yellow channel).

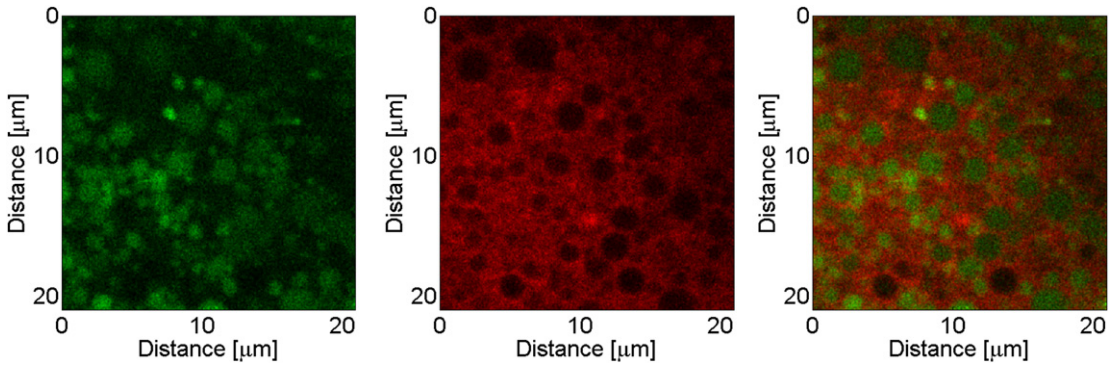

Figure 3. Spatial distribution of a luminal (Fluo-5N AM in the green channel) and a cytosolic dye (Rhod-2 in the red channel) inside the oocyte. The third image shows the superimposed fluorescence of both channels.

bound to dye around the release site which causes the fluorescence to decrease. The control oocyte rules out the hypothesis that the UV light affects the fluorescence of Fluo-5N AM.

3.2. Stationary distribution of cytosolic and luminal dyes

We show in figure 2 images obtained after having micro injected the oocytes with Fluo-4 and Rhod-2 dextran, two dyes that remain in the cytosol. The two channels are superimposed in the third image.

Both dyes present similar staining patterns inside the oocyte. They both diffuse in the cytosol and fluoresce when bound to Ca^{2+}, so that their fluorescence comes from the same region. The dark regions observed in all three images correspond to regions where the dyes cannot enter, either cortical or pigment granules or intracellular organelles. To quantify the colocalization between the two dyes, we calculated the Pearson correlation coefficient obtaining a value of 0.44. This value might seem low but we should keep in mind that this type of computation provides a linear comparison. Fluo-4 and Rhod-2 have very different dissociation constants, 770 nM and 2000 nM respectively. While we might expect that, under basal conditions, Rhod-2 is linearly proportional to free Ca^{2+}, this condition does not necessarily hold for Fluo-4. This would introduce a nonlinear dependence between both fluorescence distributions that could result in the coefficient that we obtained.

The same imaging experiment was performed but with Fluo-5N AM and Rhod-2. The images obtained are shown in figure 3. Fluorescence from the Fluo-5N AM channel has a different spatial distribution than fluorescence from the Rhod-2 channel. Rhod-2, as in the previous experiment, is labeling cytosolic Ca^{2+} while Fluo-5N AM seems to be probing Ca^{2+} in a different reservoir. In this case, the Pearson correlation coefficient is -0.017 indicating that there is no correlation between both images. In the superimposed image of both channels some of the structures that appear as dark circles in the Rhod-2 channel are bright in the Fluo-5N AM channel almost as if the spatial distribution of the dyes was complementary in those regions. These results and those of the previous subsection suggest that Fluo-5N AM is not staying in the cytosol but probing Ca^{2+} in a different reservoir.

3.3. Labeling the ER

We show in figure 4 images obtained after having micro injected the oocytes with Fluo-5N AM and Dil, a lipophilic tracer that labels intracellular membranes.

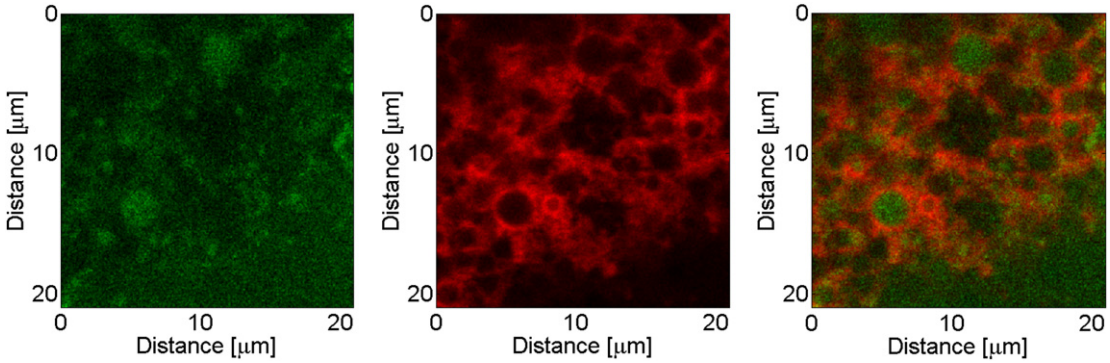

Figure 4. Spatial distribution of a luminal dye (Fluo-5N AM in the green channel) and an ER membrane tracer (Dil in the red channel) inside the oocyte. The third image is the superimposed fluorescence distribution of both channels.

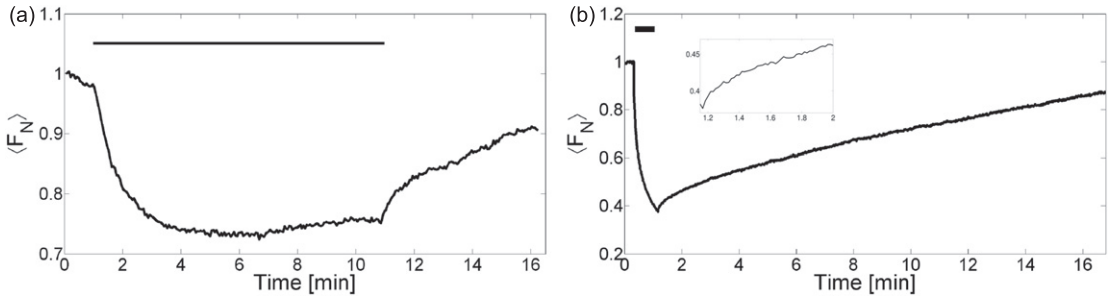

Figure 5. Monitoring luminal Ca^{2+} dynamics: time course of normalized mean Fluo-5N AM fluorescence in the presence of a UV exposure. (A) Mean fluorescence signal during a sustained stimulus (bar at the top) for [Fluo-5N AM] = 92 μM. (B) Fluorescence recovery after a short strong stimulus for [Fluo-5N AM] = 74 μM. The inset shows the initial phase of the recovery.

The Fluo-5N AM channel (green) presents large filled structures and noisy unfocused regions. Some of those regions appear connected in the image and some are isolated. The Dil channel presents a staining pattern irregular with different structures similar to those described in [33] and [34] where the same tracer is used to label the ER membrane. Some of those structures appear to enclose cylindrical (or spherical) volumes. The ER membrane is not a flat structure but is a network of tubules and cisternae that are distributed in a large cytosolic volume [35]. As was seen in the cytosolic dyes, there are dark regular structures in both channels such as granules. By looking at the superimposed image of both channels, we observe that some structures appear dark in the Dil channel but are bright in the Fluo-5N AM channel. Dil seems to be labeling the border of such structures while Fluo-5N AM seems to be labeling their interior. For the images shown in figure 4 the Pearson correlation coefficient is $P = 0.057$. This indicates that there is no correlation between the fluorescence in the Fluo-5N AM channel and the fluorescence in the Dil channel. The two dyes do not colocalize inside the oocyte, Dil is staying on the ER membrane (a 2D structure) while Fluo-5N AM is bound to Ca^{2+} inside a 3D reservoir that seems to be enclosed by this membrane.

The images of figure 4 are also used to estimate the surface to volume ratio of the ER. Applying a threshold we estimated the number of pixels of the image that correspond to the ER membrane and to the ER lumen. Assuming that the intersection of the ER surface and its lumen with the image plane are one and two dimensional, respectively, we consider that the fraction of pixels that corresponds to each of these regions can be used to estimate the area to volume ratio of the ER (in pixels). Considering further that the ER membrane pixels are overestimated because the lateral resolution of the microscope is 4 times larger than our pixel size we divide that number by 4. In this way we obtain a $\sim 1/5$ ratio of surface to volume in pixels that corresponds to a ~ 5 μm^{-1} surface to volume ratio.

3.4. Luminal and cytosolic Ca^{2+} dynamics

In the previous sections we provided solid proof that Fluo-5N AM is labeling Ca^{2+} inside the ER. In this section we use it to study the dynamics of luminal $[Ca^{2+}]$ during the release of Ca^{2+} through IP_3Rs. In all these experiments we use caged $InsP_3$ that we photorelease with a UV exposure to elicit a Ca^{2+} signal and obtain sequences of frames. We then compute the mean fluorescence over the whole frame, $\langle F \rangle$ as a function of time. We show in figure 5(a) the normalized mean fluorescence $\langle F_N \rangle$ derived from an experiment in which we only used the dye, Fluo-5N AM. The

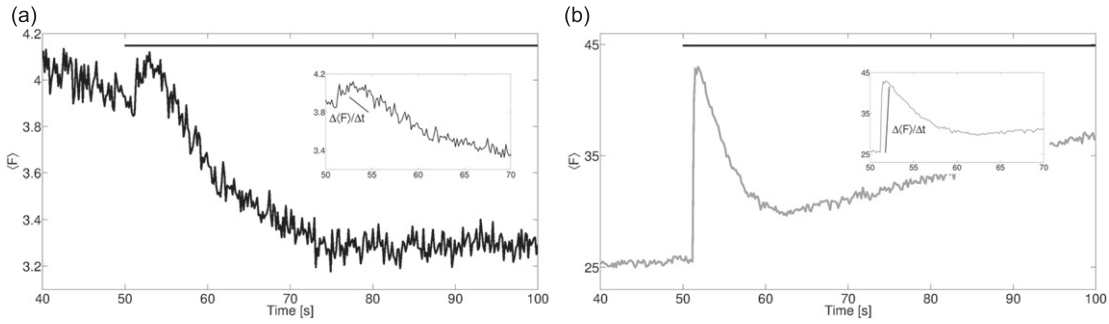

Figure 6. Time courses of the fluorescence in the Fluo-5N AM (luminal dye) and Rhod-2 (cytosolic dye) channels during a sustained photo release of caged $InsP_3$. The black bar at the top indicates the UV uncaging stimulus. (A) $\langle F\rangle$ for Fluo-5N AM during the early stages of the release, the inset shows how we estimated $\Delta\langle F\rangle/\Delta t$. (B) $\langle F\rangle$ for Rhod-2 during the early stages of the release, the inset shows how we estimated $\Delta\langle F\rangle/\Delta t$ in this case.

9 min long UV exposure is indicated with a bar at the top. We observe that the fluorescence decreases abruptly after the UV illumination starts and then remains almost constant (and slightly increasing) at approximately 70% of its initial value while the UV illumination is still on. The fluorescence starts to recover immediately after the UV light is turned off. We also performed experiments where the stimulus was a more powerful but shorter UV exposure. We show in figure 5(b) the normalized mean fluorescence as a function of time for such an experiment. There we observe that during the UV stimulus $\langle F\rangle$ decreases reaching~40% of its initial value just before the UV illumination is turned off. After that, the fluorescence starts to recover. This recovery presents two phases, the initial one appears to be faster and exponential and the following phase is slower and linear. The signal recovery is much slower than the $InsP_3$ induced depletion. The time course of the signals shown in figure 5 reflects the behavior of the entire scanned region.

The 30% variation in $\langle F_N\rangle$ depicted in figure 5(a) does not seem to be equivalent to the changes that are usually obtained during Ca^{2+} signals when observed from the cytosolic side. In order to analyze this better we performed a series of experiments where we monitored simultaneously Fluo-5N AM and Rhod-2 during long UV exposures of different intensities. We performed this type of experiments 37 times in 10 different oocytes, most of them with a low intensity UV exposure. We show in figure 6 one of these experiments. In this case we plot the mean fluorescence, $\langle F\rangle$, obtained in the Fluo-5N AM channel (figure 6(a)) and the corresponding one in the Rhod-2 channel (figure 6(b)). The black bars at the top represent the UV exposure that is turned on approximately 50 s after the acquisition begins and is then left on for the rest of the experiment. We observe much more moderated changes in the Fluo-5N AM than in the Rhod-2 fluorescence (notice the different scales of the plots). We also observe that after its initial elevation, the Ca^{2+}-bound Rhod-2 fluorescence eventually decreases even though caged $InsP_3$ is still being photo-released and luminal calcium is decreasing as well. Furthermore, for long enough times in certain experiments the dynamics of Ca^{2+}-bound Rhod-2 and Ca^{2+}-bound Fluo-5N AM are even qualitatively different (see Supporting Material). Both behaviors can be due to calcium exchange with regions outside the one that is being imaged. While we may assume that there is exchange with these other regions, it is unlikely that this spatial coupling occurs very soon after the initiation of the UV photo-release. Therefore, during these early stages after the start of the UV pulse we may compare the variation in the Rhod-2 and the Fluo-5N AM channels using the model presented in section 2.6. In order to advance towards a quantitative comparison of the Ca^{2+} variations in the cytosol and the lumen immediately after the UV stimulus starts we compute $\Delta\langle F\rangle/\Delta t$ for the Fluo-5N AM and the Rhod-2 signals of the 37 experiments over the short time interval over which the Rhod-2 signal increases. We also compute $\langle F_b\rangle$ before the UV exposure for the two dyes. After pooling all the data for each dye we compute the mean over all the values obtained and derive the estimates $\frac{1}{\langle F_b\rangle}\frac{\Delta\langle F\rangle}{\Delta t}|_{R2} = 1.5\ s^{-1}$ and $\frac{1}{\langle F_b\rangle}\frac{\Delta\langle F\rangle}{\Delta t}|_{F5} = -0.0023\ s^{-1}$ for Rhod-2 and Fluo-5N AM, respectively. We then use 11 to obtain the time variations of $\langle[CaD]\rangle$ for each dye. Using the parameters described in section 2.6 we obtain, for the cytosol (i.e. from the Rhod-2 signal), $\frac{\Delta\langle[CaD^c]\rangle}{\Delta t}|_{rel} = 12.6\ \mu M\ s^{-1}$. In order to derive an estimate for the variation in total Ca^{2+} from $\Delta\langle[CaD^c]\rangle$ we consider two extreme cases: an unrealistic one in which $\Delta\langle[CaD^c]\rangle = \Delta[Ca_T^{(c)}]$ and a more realistic one in which $\Delta\langle[CaD^c]\rangle = 0.08\Delta[Ca_T^{(c)}]$. The latter estimate corresponds to assuming that there is a cytosolic buffer of $K_D \sim 250$ nM at a 300 μM concentration [36] (see Supporting Material). In this way the

total cytosolic [Ca^{2+}] time variation is restricted by

$$12.6\ \mu\text{M s}^{-1} \leqslant \frac{\Delta\langle[\text{Ca}_T^c]\rangle}{\Delta t}|_{\text{rel}} \leqslant 158\ \mu\text{M s}^{-1}. \quad (13)$$

Approximating $\Delta/\Delta t \approx \partial/\partial t$ and inserting 13 into 10 we obtain

$$-\frac{V_c}{V_L}158\ \mu\text{M s}^{-1} \leqslant \frac{\Delta\langle[\text{CaD}^{(L)}]\rangle}{\Delta t}|_{\text{rel}} + \frac{\Delta}{\Delta t}(\langle[\text{Ca}^L]\rangle + \langle[\text{CaB}^L]\rangle)|_{\text{rel}} \leqslant -\frac{V_c}{V_L}12.6\ \mu\text{M s}^{-1}. \quad (14)$$

In order to repeat the calculation that led to 13 for the case of luminal Ca^{2+} and Fluo-5N AM we find one difficulty: the total dye concentration cannot be estimated as easily because we are not certain of what fraction of the injected Fluo-5N AM has effectively entered the lumen. An upper bound for the luminal total dye concentration, $[D_T^L]$, can be estimated in terms of the total intracellular concentration, [Fluo-5N AM] =15 μM, as

$$[D_T^L] \leqslant [\text{Fluo–5N AM}]\left(1 + \frac{V_{cT}}{V_{LT}}\right), \quad (15)$$

with V_{LT} and V_{cT} the luminal and cytosolic volumes, provided that Fluo-5N AM does not enter intracellular stores other than the ER. Counting the total number of fluorescent pixels in the Rhod-2 and the Fluo-5N AM channels of the images analyzed in this section we can estimate the ratio of the luminal (V_L) to cytosolic (V_c) volume in the observed region (see Supplementary Material for details). In this way we obtain $\frac{V_c}{V_L} = 1.4$. Even though the experimental images were obtained in a region where the ER may be over-represented we still use $[\text{Fluo5N} - \text{AM}]\left(1 + \frac{V_c}{V_L}\right)$ as an upper bound estimate of the total concentration of the dye in the lumen. We obtain $[D_T^L] \leqslant 36\ \mu$M. Proceeding as in the case of the Rhod-2 channel we obtain a bound for the Ca^{2+}-bound dye variation in the lumen during the initial stages of the Ca^{2+} release which, since this variation is negative, it is

$$-0.06\ \mu\text{M s}^{-1} \leqslant \frac{\Delta\langle[\text{CaD}^L]\rangle}{\Delta t}|_{\text{rel}} \leqslant 0. \quad (16)$$

Inserting this estimate and $\frac{V_c}{V_L} = 1.4$ in (14) we conclude that $\Delta\langle[\text{CaD}^L]\rangle/\Delta t$ is negligible compared to $\Delta(\langle[\text{Ca}^L]\rangle + \langle[\text{CaB}^L]\rangle)/\Delta t$.

4. Discussion and conclusions

4.1. Fluo-5N AM probes luminal Ca^{2+} in *Xenopus laevis* oocytes

The dye Fluo-5N AM was previously used to probe luminal Ca^{2+} in muscle fibers of the cane toad [37], cardiac myocytes [38], astrocytes [39] and in pancreatic acinar cells [40] among others. This is the first time that this indicator is used in *Xenopus laevis* oocytes. We performed different controls to check its efficiency. First, we evaluated its intracellular loading (see figure 1(a)). We compared the final fluorescence of the indicator in the presence of different cytosolic buffers (see figures S2A and S2B of the Supplementary Material) and showed that large concentrations of the buffers did not affect the fluorescence coming from the indicator. We concluded that, under stationary conditions, Fluo-5N AM was not reporting the distribution of Ca^{2+} in the cytosol but in some other intracellular store. This is consistent with what we expected based on the high K_D of Fluo-5N AM [38]. We also performed experiments with caged $InsP_3$ and showed that the Fluo-5N AM fluorescence decreased immediately after the photo-release of the caged $InsP_3$ started and that it recovered as soon as the photo-release was turned off (see figure 5). We also ruled out that the decrease in the Fluo-5N AM fluorescence in the presence of the UV illumination was due to photobleaching by performing control uncaging experiments with and without caged $InsP_3$: the decrease was observable in the former but not in the latter (see figure 1(b)). These observations led us to conclude that Fluo-5N AM was labeling Ca^{2+} inside a store from which the ions could be released through IP_3Rs, i.e., that it was labeling luminal Ca^{2+}. Then, we compared the spatial distribution of Fluo-5N AM with that of cytosolic dyes (see figures 2 and 3) and an ER membrane tracer (see figure 4). From a comparison of their localization we were able to demonstrate that the Fluo-5N AM fluorescence did not come from the cytosol or from the ER membrane but from the lumen of the ER.

4.2. ER structure in *Xenopus laevis* oocytes

The images obtained labeling both the lumen and the membrane of the ER show that in *Xenopus laevis* oocytes this reservoir has a considerable volume. The staining pattern of Dil and that of the luminal indicator do not colocalize, Dil labels the surface of the ER while Fluo-5N AM labels its internal volume. The use of both indicators simultaneously gives the possibility to obtain information about the shape of the ER and its morphology in oocytes. In these cells the ER has a significant volume and is not just a network of connected membranes. From our observations we estimated that some of the structures have a cylindrical shape with a mean diameter of 2 μm. We estimated the surface to volume ratio of the ER in the oocytes to be $\sim$1/5 (in pixels). As we will discuss in section 4.4 the morphological properties of the reservoir will shape the dynamics of luminal Ca^{2+} and will influence the type of events that can arise.

4.3. Estimation of Ca^{2+} fluxes and the role of luminal buffers

After proving that Fluo-5N AM was a viable luminal Ca^{2+} indicator, we used it to investigate the dynamics of luminal Ca^{2+} during global events. We first performed experiments in which only the dye

Fluo-5N AM was used (figure 5). These experiments showed that the decrease in the Ca^{2+}-bound Fluo-5N AM concentration was relatively small compared to the changes that are usually observed in cytosolic dyes during Ca^{2+} release events. This occurred even in experiments with very strong UV exposures (figure 5(b)). In order to investigate this further, we then performed experiments with Fluo-5N AM and a cytosolic dye, Rhod-2, monitoring the fluorescence coming from both dyes simultaneously. From the analysis of the experiments we obtained lower and upper bounds for the total $[Ca^{2+}]$ variation in the cytosol (see 13) and a lower bound for the [CaD] variation in the lumen (see 16) which led us to the conclusion that $|\Delta\langle[CaD^L]\rangle/\Delta t| \ll |\Delta(\langle[Ca^L]\rangle + \langle[CaB^L]\rangle)/\Delta t|$. We now argue that the latter is dominated by the Ca^{2+}-bound buffer term. To this end we estimate $\frac{\Delta\langle[Ca^L]\rangle}{\Delta t}$. A fast calculation can be performed assuming that Ca^{2+} and CaD are in equilibrium in the lumen at all times:

$$[Ca^L] = K_D \frac{\frac{[CaD^L]}{[D_T^L]}}{1 - \frac{[CaD^L]}{[D_T^L]}}, \tag{17}$$

so that

$$\frac{\Delta\langle[Ca^L]\rangle}{\Delta t} = \frac{K_D}{[D_T^L]} \frac{\Delta\langle[CaD^{(L)}]\rangle}{\Delta t} \left(\frac{1}{1 - \frac{[CaD^L]}{[D_T^L]}}\right)^2. \tag{18}$$

With the numerical values derived in section 3.4 we obtain $\frac{\Delta\langle[Ca^L]\rangle}{\Delta t} = -1.5\ \mu M\ s^{-1}$ which, in absolute value, is much smaller than the bounds imposed by 14. In any case, inserting this estimate in 14 we arrive at:

$$-219\ \mu M\ s^{-1} \leqslant \frac{\Delta\langle[CaB^L]\rangle}{\Delta t} \leqslant -16.1\ \mu M\ s^{-1}. \tag{19}$$

This decrease in Ca^{2+}-bound buffer results in a net free Ca^{2+} influx inside the ER. Considering one (effective) luminal buffer it is:

$$\frac{\Delta\langle[CaB^L]\rangle}{\Delta t} \approx k_{on}^B [Ca^L][B^L] - k_{off}^B [CaB^L], \tag{20}$$

where we assume that during the early stages of the release, the dominating term is $k_{off}^B[CaB^L]$. In this way we can have an estimation of the magnitude of this term:

$$\frac{\Delta\langle[CaB^L]\rangle}{\Delta t} \sim -k_{off}^B [CaB^L]. \tag{21}$$

Using the basal estimates, $[Ca^L] = 200\ \mu M$ and $[Ca_T^L] = 1$ mM [41], we obtain $[CaB^L] = 800\ \mu M$ which, in combination with 19–21, gives $0.02\ s^{-1} \leqslant k_{off}^B \leqslant 0.3\ s^{-1}$ (the upper bound corresponds to the realistic case in which $\Delta\langle[CaD^c]\rangle = 0.08\Delta[Ca_T^{(c)}]$). This off rate is relatively small but is perfectly compatible with having a Ca^{2+} buffer of small dissociation constant (as the ones proposed in [31]) that could act as a large Ca^{2+} repository in the lumen. Thus, it is the large buffer concentration that can account for a (fast) release of free Ca^{2+} in the lumen that can rapidly help overcome the luminal Ca^{2+} depletion during IP_3R-mediated Ca^{2+} release events.

To test the consistency of our model, we can estimate the flux through the IP_3Rs and obtain a value for the amount of open receptors during a release in our scanned region. From 9 we have

$$\frac{\Delta\langle[Ca_T^{(c)}]\rangle}{\Delta t}\Big|_{rel} \approx \frac{1}{V_c}\left(\int_A \vec{j}_{IP_3R} \cdot \vec{dS}\right) = \frac{I_{IP_3R} N_{IP_3R}}{V_c q_{Ca}}, \tag{22}$$

where the flux through the open receptors can be written in terms of of the current through one open receptor, $I_{IP_3R} \sim 0.1$ pA, the charge of a Ca^{2+} ion, q_{Ca}, and the number, N_{IP_3R}, of simultaneously open receptors on the ER-cytosol exchange area, A. Combining (13) and (22), we can estimate bounds for the number N_{IP_3R}.

$$15 \leqslant N_{IP_3R} \leqslant 184. \tag{23}$$

To estimate the volume V_c of the cytosol in our scanned region, we consider that 36% of the total pixels of the image are cytosolic pixels (see Supplementary Material for details) and that fluorescence in a pixel comes from a volume that can be calculated using the pixel size (lateral resolution) and the approximate axial resolution of 1 μm for a confocal microscope. To estimate the area of the ER in the scanned region we first estimate the number of luminal pixels. With this estimation and the surface to volume ratio for the ER in pixels, we can calculate the number of pixels in the image that correspond to the ER membrane. We estimate that the ER surface in our scanned region is 200 μm^2. Given that the estimated mean distance between IP_3R clusters on the surface of the ER in *Xenopus laevis* oocytes is 2 μm [8], on a 200 μm^2 area there could be ~50 IP_3R clusters. This in turn results, on average, in between 0.3 (for our unrealistic case in which $\Delta\langle[CaD^c]\rangle = \Delta[Ca_T^{(c)}]$) and 4 (for the more realistic one in which $\Delta\langle[CaD^c]\rangle = 0.08\Delta[Ca_T^{(c)}]$) simultaneously open receptors per cluster which is a reasonable number [12, 42].

4.4. Summary and conclusions

Luminal Ca^{2+} plays a key role shaping the dynamics of intracellular Ca^{2+} signals that are mediated by RyRs [19–21, 28]. For this type of signals luminal Ca^{2+} is directly involved in the termination of the elementary release events known as *sparks*. In fact, there is an observable local luminal Ca^{2+} depletion (a *blink*) in the vicinity of an open RyR [28] that can decrease the open probability of the channels and also lead to a smaller single-channel current. The role of luminal Ca^{2+} on the kinetics of IP_3Rs and of IP_3R-mediated Ca^{2+} signals has not been studied in that much detail. In this paper we investigated the dynamics of luminal Ca^{2+} during IP_3R-mediated release events using the

Xenopus laevis oocyte as a model system. Besides having shown that we could indeed monitor luminal Ca^{2+} in this cell type using Fluo-5N AM we also quantified the area to volume ratio of the ER and the rate at which the concentration of luminal Ca^{2+} changes during the release through IP_3Rs while simultaneously quantifying changes in cytosolic Ca^{2+}. The observations are compatible with the existence of a relatively fast refilling mechanism that can preclude the depletion of luminal Ca^{2+} even at a local level. This is different from the observations in myocytes where blinks could be detected [28]. This difference is likely to be a consequence of the larger area to volume ratio of cardiomyocytes compared to the ratio we estimated in *Xenopus laevis* oocytes. We now quantify what implications this different area to volume ratio can have on the local depletion of luminal Ca^{2+}. To this end, we consider that the typical width of a blink estimated in [28], ~740 nm, gives an idea of how far the depleted region of the lumen extends along a direction parallel to the SR membrane. This depletion occurs in cisternae with an internal width of ~30 nm, much smaller than the lateral range of the depleted region. Thus, we approximate the depleted volume inside the lumen by a cylinder of a 740 nm diameter and a 30 nm height. If there is any refilling of Ca^{2+} into this region from the lumen of the SR, the corresponding flux should go through the lateral area of the cylinder which measures ~0.07 μm^2. If we consider a similar (circular) area of depletion parallel to the ER membrane in the case of the oocyte, since the tubules of the lumen have a ~1 μm radius, which is larger than 740 nm, we can assume that the depleted volume in this case be half a sphere of with a 740 nm diameter. In this case the refilling flux from the lumen would enter the depleted region through the surface of this half sphere which measures ~0.86 μm^2, i.e., 12 times larger than in the case of the cardiomyocyte. Furthermore, this simple calculation shows why there always seems to be more luminal Ca^{2+} available in the case of the oocyte something that could probably be relevant for physiological purposes. We then conclude that also from the luminal side the interplay between geometry and dynamics plays a relevant role on the intracellular Ca^{2+} signals that can be elicited and detected.

Being able to analyze and quantify the dynamics of luminal Ca^{2+} during IP_3R-mediated Ca^{2+} signals directly from observations has many potential applications. On one hand, monitoring luminal Ca^{2+} can give hints on whether it is involved in signal termination. On the other hand, these studies can help advance determining to what extent luminal Ca^{2+} may provide the global negative feedback that is apparently taking place when IP_3R-mediated Ca^{2+} signals embrace the whole cell (e.g., during Ca^{2+} spikes) [43, 44]. This last aspect is most relevant to understand the way in which the frequency-encoding of Ca^{2+} signals works. Based on the studies of our paper, free luminal Ca^{2+} seems to be almost always available so that the answer to these two questions apparently is negative. We understand that our studies constitute only a first step that need further validation. We plan to further advance in this regard particularly by looking at how the spatial distribution of both luminal and cytosolic Ca^{2+} is implicated in the dynamics of this universal signaling agent.

Acknowledgments

We thank Lorena Sigaut and Darío Kunik for useful discussions. This research has been supported by UBA (UBACyT 20020130100480BA), ANPCyT (PICT 2013-1301 and PICT 2010-2767). SPD is a member of Carrera del Investigador Científico (CONICET).

Author Contribution LFL designed and performed research, analyzed data and wrote the paper. SPD designed research, contributed analytic tools and wrote the paper.

References

[1] Berridge M J, Bootman M D and Lipp P 1998 Calcium—a life and death signal *Nature* **395** 645–8
[2] David E 2007 Clapham calcium signaling *Cell* **131** 1047–58
[3] Taylor C W and Laude a J 2002 IP 3 receptors and their regulation by calmodulin and cytosolic Ca^{2+} *Cell Calcium* **32** 321–34
[4] Foskett J K, White C, Cheung K-h and Mak D o D 2007 *Physiol. Rev.* **87** 593–658
[5] Choe C-U and Ehrlich B E 2006 The inositol 1, 4, 5-trisphosphate receptor (IP3R) and its regulators: sometimes good and sometimes bad teamwork *Sci. STKE* **2006** re15
[6] Lechleiter J D and Clapham D E 1992 Molecular mechanisms of intracellular calcium excitability in X laevis oocytes *Cell* **69** 283–94
[7] Taylor C W and Tovey S C 2010 IP3 Receptors: toward understanding their activation *Cold Spring Harb. Perspect. Biol. Perspect. Biol.* **2** a004010
[8] Sun X P, Callamaras N, Marchant J S and Parker I 1998 *J. Physiol.* **509** 67–80
[9] Dupont G, Combettes L, Bird G S and Putney J W 2011 Calcium oscillations *Cold Spring Harb. Perspect. Biol.* **3** a004226
[10] Diambra L and Marchant J S 2011 *Biophys. J.* **100** 822–31
[11] Piegari E, Sigaut L and Dawson S P 2015 Ca^{2+} images obtained in different experimental conditions shed light on the spatial distribution of IP3 receptors that underlie Ca^{2+} puffs *Cell Calcium* **57** 109–19
[12] Lopez L, Piegari E, Sigaut L and PDawson S 2012 Intracellular calcium signals display an avalanche-like behavior over multiple lengthscales *Front. Physiol.* **3** 1–3
[13] Callamaras N and Parker I 2000 Phasic characteristic of elementary Ca(2+) release sites underlies quantal responses to IP(3) *EMBO J.* **19** 3608–17
[14] Dargan S L and Parker I 2003 Buffer kinetics shape the spatiotemporal patterns of IP3-evoked Ca^{2+} signals *J. Physiol.* **553** 775–88
[15] Camacho P and Lechleiter J D 1993 Increased frequency of calcium waves in Xenopus laevis oocytes that express a calcium-ATPase *Science* **260** 226–9
[16] Irvine R F 1990 'Quantal' Ca^{2+} release and the control of Ca^{2+} entry by inositol phosphates-a possible mechanism *FEBS Lett.* **263** 5–9
[17] Fraiman D and Dawson S P 2004 A model of the IP3 receptor with a luminal calcium binding site: Stochastic simulations and analysis *Cell Calcium* **35** 403–13

[18] Yamasaki-Mann M, Demuro A and Parker I 2010 Modulation of endoplasmic reticulum Ca^{2+} store filling by cyclic ADP-ribose promotes inositol trisphosphate (IP3)-evoked Ca^{2+} signals *J. Biol. Chem.* **285** 25053–61
[19] Terentyev D, Viatchenko-Karpinski S, Valdivia H H, Escobar A L and Györke S 2002 Luminal Ca^{2+} controls termination and refractory behavior of Ca^{2+}-induced Ca^{2+} release in cardiac myocytes *Circ. Res.* **91** 414–20
[20] Györke S, Györke I, Lukyanenko V, Wiesner T F and Viatchenko-karpinski S 2002 Regulation of sarcoplasmic reticulum calcium release by luminal calcium in cardiac muscle *Front. Biosci.* **7** 1354–63
[21] Chen W *et al* 2014 The ryanodine receptor store-sensing gate controls Ca^{2+} waves and Ca^{2+}-triggered arrhythmias *Nat. Med.* **20** 184–92
[22] Sienaert I, De Smedt H, Parys J B, Missiaen L, Vanlingen S, Sipma H and Casteels R 1996 Characterization of a cytosolic and a luminal Ca^{2+} binding site in the type I inositol 1,4,5-trisphosphate receptor *J. Biol. Chem.* **271** 27005–12
[23] Higo T, Hattori M, Nakamura T, Natsume T, Michikawa T and Mikoshiba K 2005 Subtype-specific and ER lumenal environment-dependent regulation of inositol 1,4,5-trisphosphate receptor type 1 by ERp44 *Cell* **120** 85–98
[24] Ludwig Missiaen B Y, Taylor C W and Berridge M J 1992 Luminal Ca^{2+} Promoting Spontaneous Ca^{2+} Release from Inositol Trisphosphate-Sensitive Stores in Rat Hepatocytes *J. Physiol.* **455** 623–40
[25] Vais H, Foskett J K, Ullah G, Pearson J E and Mak D-O D 2012 Permeant calcium ion feed-through regulation of single inositol 1,4,5-trisphosphate receptor channel gating *J. Gen. Physiol.* **140** 697–716
[26] Paredes R M, Etzler J C, Watts L T, Zheng W and Lechleiter J D 2008 Chemical calcium indicators *Methods* **46** 143–51
[27] Sigaut L, Barella M, Espada R, Ponce M L and Dawson S P 2011 Custom-made modification of a commercial confocal microscope to photolyze caged compounds using the conventional illumination module and its application to the observation of Inositol 1,4,5-trisphosphate-mediated calcium signals *J. Biomed. Opt.* **16** 066013
[28] Brochet D X P, Yang D, Di Maio A, Lederer W J, Franzini-Armstrong C and Cheng H 2005 Ca^{2+} blinks: rapid nanoscopic store calcium signaling *Proc. Natl Acad. Sci. USA* **102** 3099–104
[29] Piegari E, Lopez L, Perez Ipiña E and Dawson S P 2014 Fluorescence fluctuations and equivalence classes of Ca^{2+} imaging experiments *PLoS One* **9** e95860
[30] Kelly S M, Butler J P and Macklem P T 1995 Control of cell volume in oocytes and eggs from Xenopus laevis *Comp. Biochem. Physiol.—Physiol.* **111** 681–91
[31] Baran I 2003 Integrated luminal and cytosolic aspects of the calcium release control *Biophys. J.* **84** 1470–85
[32] Robin G, Berthier C and Allard B 2012 Sarcoplasmic reticulum Ca 2 + permeation explored from the lumen side in mdx muscle fibers under voltage control *J. Gen. Physiol.* **139** 209–18
[33] Callamaras N and Parker I 1999 Radial localization of inositol 1,4,5-trisphosphate-sensitive Ca^{2+} release sites in Xenopus oocytes resolved by axial confocal linescan imaging *J. Gen. Physiol.* **113** 199–213
[34] Mehlmann L M, Terasaki M, Jaffe L a and Kline D 1995 Reorganization of the endoplasmic reticulum during meiotic maturation of the mouse oocyte *Dev. Biol.* **170** 607–15
[35] Terasaki M, Runft L L and Hand a R 2001 Changes in organization of the endoplasmic reticulum during Xenopus oocyte maturation and activation *Mol. Biol. Cell* **12** 1103–16
[36] Schwaller B 2010 Cytosolic Ca^{2+} buffers *Cold Spring Harbor Perspectives in Biology* **2** a004051
[37] Kabbara A A and Allen D G 2001 The use of the indicator fluo-5N to measure sarcoplasmic reticulum calcium in single muscle fibres of the cane toad *J. Physiol.* **534** 87–97
[38] Shannon T R, Guo T and Bers D M 2003 Ca^{2+} scraps local depletions of free $[Ca^{2+}]$ in cardiac sarcoplasmic reticulum during contractions leave substantial Ca^{2+} reserve *Circ. Res.* **93** 40–5
[39] Jaepel J and Blum R 2011 Capturing ER calcium dynamics *Eur. J. Cell Biol.* **90** 613–9
[40] Gerasimenko J V, Petersen O H and Gerasimenko O V 2014 Monitoring of intra-ER free Ca^{2+} *Wiley Interdiscip. Rev. Membr. Transp. Signal* **3** 63–71
[41] Prins D and Michalak M 2011 Organellar calcium buffers *Cold Spring Harb. Perspect. Biol.* **3** 1–6
[42] Solovey G and Dawson S P 2010 Intra-cluster percolation of calcium signals *PLoS One* **5** 1–8
[43] Thurley K and Falcke M 2011 Derivation of Ca^{2+} signals from puff properties reveals that pathway function is robust against cell variability but sensitive for control *Proc. Natl Acad. Sci. USA* **108** 427–32
[44] Thurley K, Tovey S C, Moenke G, Prince V L, Meena A, Thomas A P, Skupin A, Taylor C W and Falcke M 2014 Reliable encoding of stimulus intensities within random sequences of intracellular Ca^{2+} spikes *Sci. Signa.* **7** ra59